NATIONAL ADVISORY COMMITTEE FOR AERONAUTICS

TECHNICAL NOTE 2773

AN APPROXIMATE METHOD FOR DETERMINING THE DISPLACEMENT EFFECTS AND VISCOUS DRAG OF LAMINAR BOUNDARY LAYERS IN TWO-DIMENSIONAL HYPERSONIC FLOW

By Mitchel H. Bertram

Langley Aeronautical Laboratory
Langley Field, Va.

Washington
September 1952

1C

NATIONAL ADVISORY COMMITTEE FOR AERONAUTICS

TECHNICAL NOTE 2773

AN APPROXIMATE METHOD FOR DETERMINING THE DISPLACEMENT EFFECTS AND VISCOUS DRAG OF LAMINAR BOUNDARY LAYERS IN TWO-DIMENSIONAL HYPERSONIC FLOW

By Mitchel H. Bertram

SUMMARY

A simplified approximate theory is presented by means of which the laminar boundary layer over an insulated two-dimensional surface may be calculated, a linear velocity profile being assumed, and an estimate made of its effect in changing the pressure distribution over the profile upon which the boundary layer is formed. Skin friction is also determined. Comparisons of results from this theory are made with experimental results at a Mach number of 6.86 and a Reynolds number of 980,000.

INTRODUCTION

At hypersonic speed the boundary layers at a given Reynolds number are thicker than those at lower speeds because of the large temperature gradients across the boundary layer. This thick boundary layer effectively distorts the body contours and thereby causes deviations from the pressure distributions predicted by theories which take no account of viscous effects. In the present paper, only the laminar boundary layer is considered and a theoretical method developed whereby the surface pressure distribution over either a flat plate or a two-dimensional curved surface in hypersonic flow can be obtained by taking into account the effect of the boundary layer in distorting the theoretical nonviscous flow field. This simplified analysis is based on results obtained by Busemann (ref. 1) which indicated that the velocity profile across the boundary layer formed on an insulated flat plate is approximately linear at high Mach numbers.

After the work of Busemann, Von Kármán and Tsien (ref. 2) obtained, for a flat plate, both a solution in which a linear velocity profile was assumed and a more exact solution in which the power law for viscosity with an exponent of 0.76 was used where Busemann had utilized a parabolic viscosity relationship. One of the more recent works, that

of Van Driest (ref. 3) who used the method of Crocco (ref. 4) to obtain even more exact results from a solution of the boundary-layer equations, shows that the law used to determine the viscosity variation in the boundary layer has but a small effect on the high Mach number linearity of the velocity profile.

That part of the present analysis in which the flat plate or zero pressure gradient is discussed is similar to the linear-velocity-profile analysis made by Von Kármán and Tsien but does not use the power law for viscosity, which is generally inaccurate for the range of temperature encountered at hypersonic speeds. This analysis is extended to approximate the case with pressure gradient. The case of the insulated flat plate can be solved by the more exact methods (such as that of Crocco) with little limitation as to the law of variation of the various parameters; however, these more exact solutions are laborious compared with this approximate solution and the results of the approximate solution, as will be shown, are, in general, close to the results obtained from more exact theories in predicting skin friction and displacement thickness. In most cases, the results of the more exact solutions (for example, refs. 4 and 5) are available for only limited free-stream temperatures.*

An application of this simplified theoretical analysis is presented and the results are compared with experimental surface-pressure results obtained from the Langley 11-inch hypersonic tunnel for a flat plate and a circular-arc profile set at various angles of attack to flow at a Mach number of 6.86. Also, the results of skin-friction drag obtained from the theory are compared with drag results obtained from models with wedge and diamond profiles and square plan forms.

SYMBOLS

A,B	constants in Sutherland's viscosity formula
C_f	average skin-friction drag coefficient for one side of a plate
C_D	drag coefficient
G	slope of linear $M(x)$ curve

$k \equiv \frac{\gamma - 1}{2} M^2$

*During the process of publication of this paper, a paper by Lees and Probstein (ref. 6) was published which treats the problem of the displacing effect of the boundary layer in hypersonic flow in a more rigorous manner.

L	total length along surface
M	Mach number at edge of boundary layer
M_1	Mach number in undisturbed stream
M_a	initial Mach number over surface under consideration
$N \equiv \frac{\mu_o}{P_o}\sqrt{\frac{RT_o}{\gamma}}$	
n	exponent in power law for viscosity
P	static pressure over surface
P_1	static pressure in undisturbed stream
P_2	surface local static pressure
P_o	stagnation pressure at edge of boundary layer
R	gas constant
R_e	Reynolds number based on free-stream conditions at edge of boundary layer and chord length
T	absolute temperature
T_δ	absolute temperature at edge of boundary layer
T_o	absolute stagnation temperature
u	velocity inside boundary layer and parallel to surface
U	velocity at edge of boundary layer
x	distance along surface measured from forward stagnation point
y	distance normal to surface
α	angle of attack
γ	ratio of specific heat at constant pressure to specific heat at constant volume
δ	total thickness of boundary layer

δ^*	displacement thickness of boundary layer
θ	momentum thickness of boundary layer
θ_a	initial value of momentum thickness over surface under consideration
μ_δ	dynamic viscosity at edge of boundary layer
μ_o	dynamic viscosity at wall
ρ	density inside boundary layer
ρ_δ	density at edge of boundary layer
τ_o	shearing stress at wall

THEORY

Flow Without Pressure Gradient

If flow along an insulated flat plate with a Prandtl number of unity is assumed and if the laminar boundary layer that is being formed along this plate has a linear velocity distribution normal to the plate, then the parameters of the boundary layer, as well as a good approximation to the flow field determined by the presence of the boundary layer, may be found in an uncomplicated form capable of rapid solution.

In reference 1, Busemann integrated the boundary layer for the case of laminar flow at $M = 8.8$ along an insulated flat plate for a Prandtl number of unity, constant specific heat, and a parabolic viscosity relationship obtained from the kinetic theory. Busemann found that the linear velocity profile closely approximated the exact profile obtained from these assumed conditions; thus, indications are that only small errors would result from the assumption of the linear profile. Furthermore, in reference 7, Prandtl showed that, even in the incompressible case where the boundary-layer velocity profile is more curved than at large Mach numbers, the magnitude of the displacement thickness is rather insensitive to the velocity profile chosen.

Many investigators have shown that the effect of Prandtl number on skin friction and velocity distribution in the boundary layer will be small as long as the value of the Prandtl number is near unity. Two of the more recent papers illustrating this point are references 3 and 4.

Density variation through the boundary layer.- With the assumption of no heat conduction through the boundary layer or confining wall and with a Prandtl number of unity, the energy is constant across the boundary layer. When the perfect gas law and the ordinary relation between the speed of sound and temperature are applied and the static-pressure variation through the boundary layer is assumed negligible, the density and temperature variations through the boundary layer are

$$\frac{\rho}{\rho_\delta} = \frac{T_\delta}{T} = \frac{1}{1 + \left[1 - \left(\frac{u}{U}\right)^2\right]k} \tag{1}$$

where $k \equiv \frac{\gamma - 1}{2} M^2$ and M is the Mach number at the outer edge of the boundary layer.

Displacement thickness.- The reduction of the mass flow in the boundary layer has the effect of displacing the main stream from the surface by an amount denoted by δ^*.

By definition,

$$\frac{\delta^*}{\delta} = \int_0^1 \left(1 - \frac{\rho u}{\rho_\delta U}\right) d\frac{y}{\delta} \tag{2}$$

If the density variation of equation (1) is substituted into equation (2) and a linear velocity distribution is assumed, that is

$$\frac{u}{U} = \frac{y}{\delta}$$

then equation (2) upon integration becomes

$$\frac{\delta^*}{\delta} = 1 - \frac{\log_e(1 + k)}{2k} \tag{3}$$

In figure 1, equation (3) has been plotted for a range of Mach number from 0 to 10. Of much interest and importance is the fact that at hypersonic Mach numbers the displacement thickness is almost equal to the total thickness of the boundary layer.

Momentum thickness.- The momentum loss in the boundary layer can be shown to be

$$U\int_0^{\delta}\rho u\,dy - \int_0^{\delta}\rho u^2 dy \tag{4}$$

By definition,

$$\frac{\theta}{\delta} = \int_0^1 \frac{\rho u}{\rho_\delta U}\left(1 - \frac{u}{U}\right)d\,\frac{y}{\delta} \tag{5}$$

where θ is the momentum thickness of the boundary layer. With the density variation of equation (1) and a linear velocity variation across the boundary layer, equation (5) is readily integrated to obtain

$$\frac{\theta}{\delta} = \frac{1}{k}\left[1 + \log_e\sqrt{1+k} - \sqrt{\frac{1+k}{k}}\log_e\left(\sqrt{1+k} + \sqrt{k}\right)\right] \tag{6}$$

Equation (6), because of its form, requires a high degree of accuracy in computation. A series solution of the integrand gives

$$\frac{\theta}{\delta} = \frac{1}{k}\left[\frac{k}{1+k}\frac{1}{6} + \left(\frac{k}{1+k}\right)^2\frac{1}{20} + \left(\frac{k}{1+k}\right)^3\frac{1}{42} + \cdots\right] \tag{7}$$

or

$$\frac{\theta}{\delta} \approx \frac{1}{k}\sum_{m=1}^{m=i}\left(\frac{k}{1+k}\right)^m \frac{1}{2m(2m+1)} \tag{8}$$

Equation (8) converges very rapidly at Mach numbers below about unity. Above, approximately, Mach number 3 the slow convergence of equation (8) causes the use of equation (6) to be more satisfactory from the standpoint of ease of computation where accurate tables are available. Figure 2 presents values of θ/δ as a function of Mach number for a range of Mach number from 0 to 10. The value of the ratio of the displacement thickness to momentum thickness is given as a function of Mach number in figure 3.

Though the values of δ^*/δ, θ/δ, and δ^*/θ are presented for the range of Mach number from 0 to 10, they are primarily intended for use in the range above a Mach number of approximately 4.

The values of δ^*/δ and θ/δ cannot be satisfactorily compared with results from the more exact theories because the velocity in the boundary layer asymptotically approaches the free-stream velocity. The values of δ^*/θ, however, can be compared with those predicted by more exact theories. For the incompressible case (M = 0), the values predicted by the linear velocity profile are about 15 percent high with the error diminishing as the Mach number increases.

Flow along a plane wall.- In the case where the free-stream velocity is independent of x (for example, flow along a flat plate in a gas of infinite extent), the momentum equation of the boundary layer (see ref. 8, vol. II, p. 613) is

$$\tau_o = \frac{\partial}{\partial x}\left(U\int_0^\delta \rho u\, dy - \int_0^\delta \rho u^2 dy\right) \tag{9}$$

where τ_o is the shear stress at the wall. Combining equations (5) and (9) produces

$$\tau_o = \rho_\delta U^2 \frac{d\theta}{dx} \tag{10}$$

For a laminar boundary layer with a linear velocity distribution,

$$\tau_o = \mu_o\left(\frac{\partial u}{\partial y}\right)_{y=0} = \mu_o \frac{U}{\delta} \tag{11}$$

where μ_o is the dynamic viscosity at the wall. Thus, combining equations (10) and (11) and integrating gives

$$\delta^* = \frac{\delta^*}{\delta}\left(\frac{2x}{\frac{\theta}{\delta}\frac{\rho_\delta U}{\mu_o}}\right)^{1/2} \tag{12}$$

Slope of the boundary-layer displacement-thickness curve.- Large changes in the flow field can occur when changes occur in the boundaries. Thus, the shape of the boundary layer and the angles it makes with the plane wall are of importance, particularly at hypersonic speeds where the boundary layer is extremely thick in comparison with the boundary layer at subsonic speeds at equivalent Reynolds numbers. The effective thickness of the boundary layer is considered to be the displacement

thickness and equation (12) becomes upon differentiation

$$\frac{d\delta^*}{dx} = \frac{\delta^*}{\delta}\left(2\,\frac{\theta}{\delta}\,\frac{\rho_\delta U x}{\mu_o}\right)^{-1/2} = \frac{\delta^*}{2x} \tag{13}$$

Thus, the angle of the boundary-layer displacement surface with respect to the flat plate can be determined at any point along the x-axis of the plate.

Drag of a flat plate.- If equations (11) and (12) are combined and integrated, and the definition of the mean skin-friction drag coefficient is used, then

$$C_f = 2.828\left(\frac{\theta}{\delta}\,\frac{\mu_o}{\rho_\delta U L}\right)^{1/2} \frac{P}{P_1}\left(\frac{M}{M_1}\right)^2 \tag{14}$$

for the skin-friction drag coefficient of one side of a flat plate, where P_1 and M_1 are the free-stream pressure and Mach number in the undisturbed stream before the flat plate and P and M are the pressure and Mach number in the free stream over the surface.

Equation (14) and those developed previously are not restricted to the case of the flat plate where the Mach number over the plate is the same as that in the free stream immediately before the plate; rather, this analysis may be used for a plate inclined at an angle with respect to the initial free stream as long as the flow is two-dimensional and remains laminar with no pressure gradient or separation in the region under consideration.

A plot obtained from equation (14) is given in figure 4. At a given initial Mach number, appreciable changes in the friction coefficient occur as the angle of attack is varied since the variation in the square root of the parameter $\rho_\delta U/\mu_o$ will not cancel variations in the remaining parameters, which are functions of Mach number only. An angle-of-attack variation of approximately -15° to 15° for one surface of a plate is covered for each value of undisturbed-stream Mach number M_1 in this plot.

The dashed line in figure 4, representing the case where the conditions over the plate are the same as those in the undisturbed stream, does not occur at zero angle of attack for, as shown by a consideration of equation (13), the boundary layer prevents this. The zero angle of a flat plate relative to the incident stream is thus in the region above the line for $M = M_1$.

Substituting equation (A4) of the appendix, in which Sutherland's formula is used to define the relationship between $\rho_\delta U/\mu_o$ and $\rho_\delta U/\mu_\delta$, into equation (14) yields

$$C_f = 2.828\sqrt{\frac{\theta/\delta}{R_e}}\,(1+k)^{3/4}\left(\frac{\frac{T_o}{1+k}+B}{T_o+B}\right)^{1/2}\frac{P}{P_1}\left(\frac{M}{M_1}\right)^2 \qquad (15)$$

where R_e is the Reynolds number based on free-stream conditions over the plate. If the conditions over the plate are assumed to be the same as those in the undisturbed stream and a value for Sutherland's constant is determined (see appendix), figure 5 is obtained.

In order to compare the results from equation (15) with results from the more exact theories, figure 6 has been prepared. The upper three curves in this figure were obtained from reference 3 and the lower curve was obtained from equation (15). The two curves labeled Crocco-Van Driest were obtained by Van Driest (ref. 3) using Crocco's method (ref. 4). The curve obtained by Von Kármán and Tsien by use of the power law for viscosity with an exponent of 0.76 was originally presented in reference 2. Figure 6 shows, as was pointed out previously, that variations in the Prandtl number have but a small effect on the skin friction and indicates the errors that can be incurred by using the viscosity power law instead of the more accurate Sutherland's formula. The good accuracy at hypersonic Mach numbers of results obtained by using the assumption of a linear velocity profile, as compared with the results obtained by using the more exact theories, is also shown in figure 6.

The results of an analysis by Klunker and McLean (ref. 5), which is even more exact than the work of Crocco and Van Driest, have not been included since these results would be almost coincident with the Crocco-Van Driest curve for a Prandtl number of 0.75 through the Mach number range 1 to 5 for which the calculations of reference 5 have been made.

Flow With Pressure Gradient

At the lower supersonic Mach numbers, the boundary-layer profile shape is relatively unaffected by the effects of pressure gradient as indicated by the results of reference 9. In hypersonic wind-tunnel flow, relatively large changes in Mach number result in but small changes in velocity because the maximum velocity obtainable is being closely approached. The velocity distribution across the boundary

layer on an insulated plate in the presence of a negative pressure gradient is thus assumed to be linear as was assumed for the case of no gradient of pressure. As before, the Prandtl number is assumed to be unity.

Momentum thickness of boundary layer.- For the case of steady flow with a pressure gradient, the momentum equation of the boundary layer can be written in the form

$$\frac{\tau_o}{\rho_\delta U^2} = \frac{d\theta}{dx} + \theta \frac{2 - M^2 + \frac{\delta^*}{\theta}}{M(1 + k)} \frac{dM}{dx} \tag{16}$$

where U and M are, respectively, the local velocity and the local Mach number at the edge of the boundary layer. (For more details concerning the development of eq. (16), see ref. 10, p. 22.)

The ratio δ^*/θ for air where the velocity profile is linear may be represented with excellent accuracy by the following approximate equation which represents the curve given in figure 3:

$$\frac{\delta^*}{\theta} = 0.68M^2 + 3 \tag{17}$$

Substituting equation (17) and the expression for the shearing stress from equation (11) into equation (16) yields (with $\gamma = 1.40$)

$$2N \frac{\theta}{\delta} \frac{\left(1 + \frac{M^2}{5}\right)^3}{M} = 2\theta \frac{d\theta}{dx} + 2\theta^2 \frac{25 - 1.60M^2}{M(5 + M^2)} \frac{dM}{dx} \tag{18}$$

where

$$N = \frac{\mu_o}{P_o}\sqrt{\frac{RT_o}{\gamma}}$$

Equation (18) is solvable as a linear differential equation. With a linear relationship between Mach number and distance along the surface or

$$M = Gx + M_a$$

the solution is

$$\theta^2 = \frac{2}{125}\frac{N}{G}\frac{(5 + M^2)^{6.60}}{M^{10}}\int_{M_a}^{M}\frac{\theta}{\delta}\frac{M^9 dM}{(5 + M^2)^{3.60}} + \theta_a{}^2\left(\frac{M_a}{M}\right)^{10}\left(\frac{5 + M^2}{5 + M_a{}^2}\right)^{6.60} \quad (19)$$

Similar assumptions as to velocity profile and Mach number distribution were made by Puckett in reference 10 in conjunction with a pipe friction law for turbulent flow for an approximate determination of the thickness of turbulent boundary layers in nozzles.

Values of $\int_0^M \frac{\theta}{\delta}\frac{M^9 dM}{(5 + M^2)^{3.60}}$ were obtained by a graphical integration and are given in table I and figure 7 for a range of Mach number from 0 to 10; thus, the value of the integral in equation (19) between any two limits in the range presented may be determined.

After solving for θ, the relation between δ^* and θ (eq. (17) of fig. 3) will determine the value of δ^*.

Slope of boundary-layer displacement-thickness curve.- The slope of the boundary-layer displacement-thickness curve may be written as

$$\frac{d\delta^*}{dx} = \frac{\delta^*}{\theta}\frac{d\theta}{dx} + \theta\frac{d\frac{\delta^*}{\theta}}{dx} \quad (20)$$

With equations (17) and (18), equation (20) becomes

$$\frac{d\delta^*}{dx} = \frac{\delta^*}{\delta}\frac{N}{\theta M}\left(1 + \frac{M^2}{5}\right)^3 - \frac{dM}{dx}\theta\left[\frac{\delta^*}{\theta}\frac{25 - 1.60M^2}{M(5 + M^2)} - 1.36M\right] \quad (21)$$

where the first term in equation (21) is the flat-plate solution.

Skin friction of a surface with pressure gradient.- If equations (16) and (17) are used, the mean skin-friction drag coefficient of a surface with a pressure gradient can be written as

$$C_f = \frac{2}{L}\left[\int_0^{\theta}\frac{P}{P_1}\left(\frac{M}{M_1}\right)^2 d\theta + \int_{M_a}^{M}\frac{P}{P_1}\left(\frac{M}{M_1}\right)^2\theta\frac{25 - 1.60M^2}{M(5 + M^2)}dM\right] \quad (22)$$

where, as before, P_1 and M_1 are the pressure and Mach number in the undisturbed stream and P and M are the local pressure and Mach number in the stream at the edge of the boundary layer.

By utilizing equation (19) in a nondimensional form, equation (22) was evaluated for $M_1 = 4.00$ and 6.86 (the Mach number of the Langley 11-inch hypersonic tunnel) and various values of Mach number immediately following the shock at the leading edge of a curved plate M_a, the Mach number variation from the leading edge of the airfoil to the trailing edge being assumed linear. The results showed large increases in the skin friction for a surface with a Mach number gradient compared with a flat surface at zero inclination to the flow as illustrated in figure 8.

Method of Calculating Effect of Boundary Layer on Surface Pressures

Flat plate.- In the presence of boundary layer, the Mach number varies chordwise along a flat plate because of the varying slope of the effective or displacement boundary-layer thickness (from eq. (13)). The use of the actual Mach number variation along the plate was felt to be an unnecessary complication; instead, the conditions where the average angular slope of the boundary layer occurred (the quarter-chord point) were chosen to represent the conditions over the entire plate for the purpose of calculating a boundary-layer profile.

A boundary-layer displacement surface ($\delta^*(x)$) is calculated by using equation (12) and the calculations are based on the Mach number obtained from the inviscid theory. By adding the average angular slope

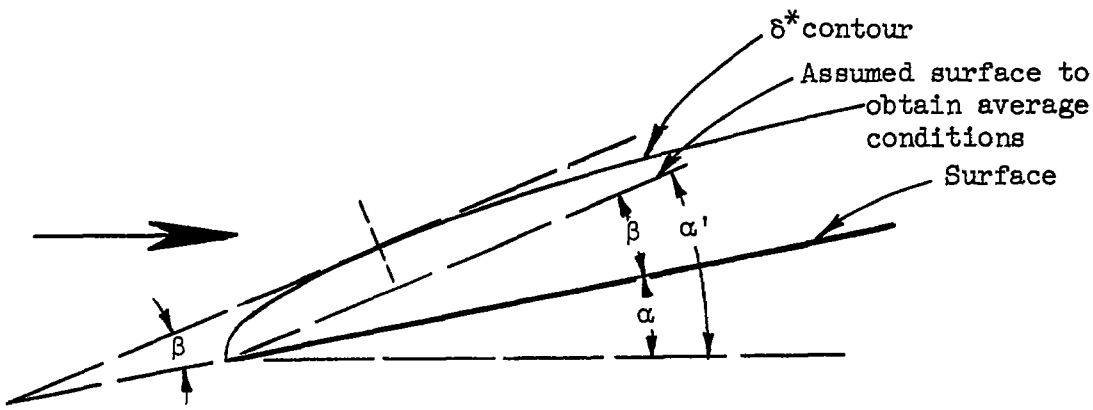

of the displacement thickness (β in the accompanying sketch) to the angle which the plate surface makes relative to the initial free stream (α) to obtain the average deflection angle of the flow (α'), the effective Mach number for computing a boundary layer for the next approximation can be found. The process is repeated until the effective Mach number agrees with the calculated profile. In this analysis, the iteration process was done very readily by means of graphs of the shock (expansion) equations and the boundary-layer displacement-thickness slopes.

The Mach number profile and, consequently, the pressure distribution is established by expanding the air downstream from the average point over the boundary-layer displacement surface and isentropically compressing the air in the upstream direction from this point. The theory, of course, is based upon the absence of such a variation in the free stream over the plate; thus, the results obtained are an approximation to the actual occurrence. The closeness of the approximation will be determined by the shape of the boundary-layer displacement surface involved.

Actually, if the Mach number determined from the inviscid theory is used to calculate a displacement surface and the slope of this surface at a given point is subtracted from the expansion angle for the inviscid-theory Mach number, the surface pressures are close to those obtained from the previous iteration process. The method of calculation by the iteration process was preferred, however, since the physical processes were more nearly duplicated. Also, the iteration procedure was not much more tedious because graphs of the various functions were used.

As the leading edge is closely approached, the slope of the boundary-layer displacement surface becomes large and the theory is invalid. The range of applicability of this method of calculating the effect of the boundary layer is restricted to small angles of the displacement profile which in itself does not restrict the solution much more than the assumptions of the orders of magnitude inherent in the boundary-layer theory.

Circular-arc surface.- With pressure gradient, a somewhat different approach is required than for a flat plate. For the determination of the flow about the circular-arc profiles used in this investigation, the assumption was first made that there was no loss in stagnation pressure over that predicted by the oblique shock theory with inviscid flow. Then, a two-step linear variation of Mach number with distance along the surface was assumed (labeled "a" in accompanying sketch)

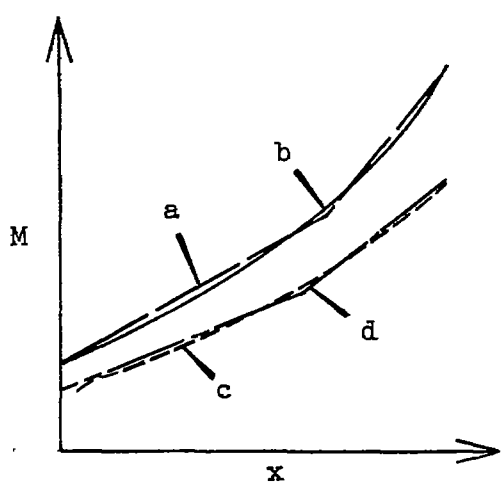

which approximated the curve obtained from the inviscid theory (b). The boundary-layer momentum thickness (eq. (19)) and the angular slope of the boundary-layer displacement profile (eq. (21)) were determined on the basis of this linear assumption. The theoretical expansion around the geometric surface was decreased by the amount of the slope of the boundary-layer displacement thickness to determine a new Mach number distribution (c) and the boundary layer was recalculated by using the linear approximation (d) to this curve. When, after successive approximations, the final iteration was closely in agreement with the final assumed curve, the mean was taken between the result of the final iteration and the Mach number variation assumed for its determination. This final Mach number variation then determined the pressure distribution over the surface when the gain in entropy was assumed to be that predicted by the oblique-shock theory with inviscid flow.

EXPERIMENT

Apparatus

Tunnel.- The tests were conducted in the Langley 11-inch hypersonic tunnel, which is a blowdown type utilizing both a high-pressure tank and a vacuum tank. The tunnel is described in references 11 and 12 and a calibration of the nozzle used for these tests is presented in reference 12. The tests in this investigation were made at an average settling-chamber pressure of 25.5 atmospheres and an average stagnation temperature of 730° F so that the Reynolds number was about 980,000 based on a 4-inch length.

Models.- Flat-plate pressure data were obtained from a wedge-shape profile and the flat side of a profile formed by a segment of a circle. Pressure data with gradient were obtained from the circular-arc surface of the segment profile. In plan form, all models were 4 inches square and had a thickness-to-chord ratio of 0.05. A photograph of one of the typical pressure models, that with the segment profile for which pressures were taken on the circular-arc surface, is shown in figure 9. These models had smooth machined surfaces with knife leading edges. Leading edges were maintained between 0.001 and 0.002 inch thick and the surfaces and edges were maintained in good condition during the series of tests by periodic polishing. Orifices, 0.040 inch in diameter and located chordwise at the midspan station, were formed by tubing which was flush with one surface and projected through the opposite surface. Additional data for the pressures on a flat surface parallel to the flow were obtained from a 20° wedge-shape model with a span of 3 inches. Pressures on one surface of this model were obtained as close as 1/8 inch from the leading edge and no farther

than $2\frac{1}{2}$ inches from the leading edge. The angle of attack of these models was set to within about 0.2°.

Two models with a 4-inch-square plan form and a 5-percent maximum thickness were used to obtain total drag data. One of these models had a wedge section and the other had a diamond section. These models, which are shown in figure 10, were attached to the support sting, which housed the force balance, by means of a cone having an included angle of 6.7° with a base of 0.5-inch diameter. The base for the diamond-section model was $1\frac{1}{2}$ inches downstream of the trailing edge and $2\frac{1}{2}$ inches downstream of the trailing edge for the wedge-section model.

Pressure recording.- Pressures over the surfaces were measured by means of the aneroid-type, six-cell manometers described in reference 11. In these instruments, the deflection of a diaphragm is converted into a rotation of a small mirror which reflects a beam of light to a moving film thereby giving a time history of the pressure. In these tests, the air expanded to as much as 60 percent below the free-stream pressure of about 0.2 inch of mercury. This lowest pressure can be measured with about 7 percent accuracy, whereas pressures of 1 inch of mercury can be measured within about one-half of 1 percent accuracy. Higher pressures were measured within 1 to 2 percent accuracy.

Schlieren.- The schlieren photograph presented in figure 11 was taken by means of the schlieren system, described in reference 11, which is of the highly sensitive double-traverse type. The photograph was taken with a flash of a few micro-seconds duration.

Errors in total drag coefficients.- The errors in total drag coefficients arise from errors in Mach number, stagnation pressure, and angle-of-attack determination and from the force-balance sensitivity. The calculated possible error that can be attributed to the cumulative effect of errors in these parameters is as follows:

C_D	ΔC_D
0.005	±0.0015
.010	±.0018
.015	±.0021
.020	±.0024

A scatter of the data that is slightly higher than this calculated error is sometimes encountered. This additional source of error is

due to the uneven heating effect of the high-stagnation-temperature air on the components of the balance.

The drag forces as measured for the two force models included the force due to the conical support and the interference effects of the support. Corrections for the drag force on the unshielded part of the conical support were applied to the total drag results. These corrections were based on calculated drag results for complete cones with limited experimental checks. No attempt was made to determine the effects of sting interference for the diamond-section model but these effects are believed to be small since the area affected by the shocks from the support constitute less than 5 percent of the model surface area.

COMPARISON OF THEORY WITH EXPERIMENT

The boundary layer was determined to be laminar by examination of its appearance in schlieren photographs. The extremely high density gradient in the outer part of the boundary layer with very little gradient near the wall makes the laminar boundary layer readily distinguishable from a turbulent boundary layer where the change in gradient is less abrupt. Also, the manner in which the boundary layer leaves the trailing edge of the airfoils is a good indication that it is laminar because very little diffusion or change in its appearance occurs as it separates from the surface near the trailing edge. Further corroboration is offered by the measured minimum drags which would be expected to be almost twice as great were the boundary layer turbulent.

In order to determine whether the surface temperatures approach the recovery temperatures closely enough so that the airfoils could be effectively considered insulated plates, the diamond-shape airfoil was tested with thermocouples imbedded flush with the airfoil surface. The angle of attack was varied from 0° to $7\frac{1}{2}^\circ$. Both the highest and lowest skin temperatures were recorded at the highest angle of attack. On the lower surface at $\alpha = 7\frac{1}{2}^\circ$ 60 seconds after the start of the test, the skin temperature was 84 percent of the stream stagnation temperature at the 7-percent-chord station, at midchord 71 percent, and at the 94-percent-chord station 73 percent of the stagnation temperature. On the upper surface at $\alpha = 7\frac{1}{2}^\circ$ at the 7-percent-chord station, the skin temperature was 80 percent of the stagnation temperature and 65 percent of the stagnation temperature at both midchord and the 94-percent station. These skin temperatures are considered sufficiently high so that only small errors result when the airfoils are considered as insulated plates.

Flat-Plate Pressure Distribution

Figure 11 presents a comparison between pressure distributions obtained from the theory (where the inviscid flow is corrected for the displacing effect of the boundary layer) and experiments in the Langley 11-inch hypersonic tunnel with a flat surface set at various angles to the incident flow. The ratio used as a parameter in this figure is a measure of the local pressure rise of the surface from the free-stream static pressure.

A very reasonable agreement between experiment and theory is seen at 0° angle of attack of the surface (fig. 11(a)) and at small angles of attack on the lower surface (fig. 11(c)). The results shown in figure 11(a) were presented by Becker in reference 13. Appreciable deviations from the theory are seen even at small angles of attack for the upper surface (fig. 11(b)), and on the lower surface the deviations from the theory become appreciable at an angle of incidence to the flow of about 8°

Various methods have been attempted to explain the discrepancy between the experimental pressures on the front part of the upper surface and the pressures predicted by the boundary-layer displacement effect. Condensation of air was ruled out since calculations, in which the oxygen component of air was assumed to condense first, showed that only at the angle of attack of 4° shown in figure 11(b) was there a possibility of even a small amount of condensation, and these calculations were made on the assumption that the full 4° expansion could be obtained.

Other calculations were made which applied the theory with pressure gradient to the upper surface, but this application of the theory with pressure gradient changed the pressures predicted by the flat-plate theory by an amount too small to explain the discrepancy.

The deviations from the theory of the results from the rear part of the upper surface are attributed largely to a relieving effect about the airfoil tips, to boundary-layer shock interaction, and to separation near the trailing edge. The pressure relieving would tend to have a much larger effect on the surface undergoing a pressure drop as compared with the opposite surface where a pressure rise is occurring. On the lower surface, only at an angle of attack of about 8° do the measured pressures start deviating from those predicted by the theory with boundary layer. Near the leading edge, the theory would not be expected to apply quantitatively but would serve only to indicate trends. The boundary layer at the leading edge can be modified by the large pressure gradient, very near the leading edge, due to the boundary-layer growth and by the pressure gradient due to leading-edge bluntness. Another modifying factor is due to the interaction of the leading-edge shock with the rapidly growing boundary layer. In addition, interaction between the various factors would be expected.

The boundary layer is shown by the schlieren photograph inserted in figure 11(a). This boundary layer deflects the main flow away from the surface so that a shock results at the leading edge followed by a high pressure which decreases with distance from the leading edge as a result of a gradual expansion after the shock. Without boundary layer, the pressure rise should be zero. A curvature to the leading-edge shock should be noted near the leading edge.

Pressure Distribution Over Circular-Arc Profile

Figure 12 presents a comparison of the pressure distributions predicted by the inviscid theory, by the theory corrected for boundary layer, and by the pressure distributions obtained experimentally at a Mach number of 6.86 at various angles of the chord of the segment profile relative to the incident air flow.

As the angles of attack increase from 0° to 6°, fair to good agreement generally exists between experiment and theory corrected for boundary layer. An increasing extent of separation as the angle of attack increases should be noticed near the trailing edge which, of course, is not predicted by this theory.

At negative angles of α, experiment, in general, shows good agreement with the corrected theory, though the pressures near the leading edge are lower than those given by the theory with boundary layer.

From these results, the boundary layer over a curved surface, such as the one tested here, seems to cause an apparent thickening and distortion of the actual surface contours. The result differs from that for a flat plate for, in this case, as the trailing edge is approached, there is an acceleration in the growth of boundary layer as the air flows from the relatively low Mach number region at the leading edge to a considerably higher Mach number near the trailing edge. This acceleration in the growth of the displacement surface of the boundary layer as the rear of the curved surface is approached occurs only at the higher local Mach numbers. Below a Mach number of about 2.6, the gradient actually tends to thin the boundary-layer displacement profile. (Refer to eq. (21).)

Drag Obtained From Theory and From Experiment

Figure 13 presents a comparison of the drag coefficients obtained from the inviscid theory, the inviscid theory with skin friction added, and the coefficients obtained from experimental data. The two-dimensional oblique-shock and expansion relations, including a correction for tip

effects from the linear theory, were used to obtain the inviscid-theory drag. For the wedge-section airfoil, a base pressure of 50 percent of free-stream pressure was used. This value was obtained from actual pressure measurements on the base of a pressure model of this airfoil. The method used for obtaining the skin-friction drag coefficient was that outlined in the theoretical section of this paper in which the flow conditions at the quarter-chord point were used to determine the boundary layer as was done in determining the effect of the boundary layer on the surface pressures.

The drag obtained from the inviscid theory was used for the form drag instead of what should be the more accurate form drag obtained from the pressures which have been corrected for displacement effect because the displacement effect on the pressure drag was small in comparison with the friction drag.

The results obtained for both the models shown in figure 13 indicate good agreement with the results obtained from the inviscid theory with skin friction added. The curve of inviscid theory alone is much lower than the experimental points; in fact, for the wedge airfoil the total minimum drag is 3.6 times the minimum drag value given by the inviscid theory, and the total minimum drag for the diamond-section wing is greater by a factor of about 3 at the test Reynolds number of about 10^6. (For more complete results on the aerodynamic characteristics of the diamond-profile square-plan-form model, see ref. 14.) Thus, at this Mach number and Reynolds number, the skin friction is evidently an important part of the drag of slender two-dimensional profiles at low angles of attack.

Similar results were also obtained from a force model of the airfoil with the circle-segment section. In this case also, good agreement existed between the experimental drag results and the results obtained from inviscid-theory drag plus skin friction in the range of angle of attack from -4° to 4°, with the theory predicting slightly higher values of total drag than the experiment outside of this range of angle of attack.

A comparison made between the average theoretical skin-friction drag of the circular-arc surface with the chord alined with the stream and a flat plate alined with the stream indicates that the skin-friction drag of the circular-arc surface is considerably higher for the test conditions. The experimental data are not accurate enough to show clearly this increase and, in general, for all the force models, are not accurate enough to show clearly the presence of the temperature effects indicated by figure 5. The data are useful, however, as a first-order check on the magnitude of the skin-friction drag predicted by theory.

CONCLUDING REMARKS

A simplified theory has been presented by means of which the compressible laminar boundary layer over a two-dimensional surface may be calculated and an estimate made of its effect in distorting the flow field about the profile upon which it is being formed. This analysis is based on viscous flow with no heat transfer where the velocity distribution across the boundary layer is linear.

Comparison of pressures obtained from the boundary-layer theory (zero pressure gradient) with experimental pressures from a flat plate at a Mach number of 6.86 has shown good agreement at zero angle of attack and at low angles of attack of the high-pressure surface. The low-pressure surface exhibits poor agreement with the theory even at low angles of attack.

Comparisons have also been made between surface pressures measured on a circular-arc profile and pressures predicted by the boundary-layer theory with the effects of pressure gradient included. Good agreement between experiment and theory is found over a wider range of angle of attack than was found for a flat plate.

The results at a Mach number of 6.86 for the drag coefficients of two 5-percent-thick square-plan-form models showed good agreement between theory with skin friction included and experiment. The values of the minimum total drag coefficients were at least three times the minimum drag coefficient predicted by the inviscid theory; thus, the skin-friction drag is evidently an important part of the low angle drag at high Mach numbers and Reynolds numbers of about 10^6.

Langley Aeronautical Laboratory
National Advisory Committee for Aeronautics
Langley Field, Va., May 26, 1952

APPENDIX

TWO LAWS FOR THE VARIATION OF VISCOSITY AND THEIR EFFECT ON THE REYNOLDS NUMBER RELATIONS

The parameter $\rho_\delta U/\mu_o$ of equation (12) may be expressed as

$$\frac{\rho_\delta U}{\mu_o} = \frac{MP}{\mu_o}\sqrt{\frac{\gamma}{R}\frac{(1 + k)}{T_o}} \tag{A1}$$

Let the viscosity at the wall be represented by Sutherland's formula

$$\mu_o = A\frac{T_o^{3/2}}{T_o + B} \tag{A2}$$

where A and B are empirical constants depending on the gas. Substituting the value of μ_o from equation (A2) into equation (A1) gives

$$\frac{\rho_\delta U}{\mu_o} = M\sqrt{\frac{\gamma}{R}(1 + k)}\,\frac{P}{A}\left(\frac{T_o + B}{T_o^2}\right) \tag{A3}$$

The wall viscosity and stagnation temperature may be replaced by the viscosity and temperature in the free stream; thus,

$$\frac{\rho_\delta U}{\mu_o} = \frac{\rho_\delta U}{\mu_\delta}\left(\frac{1}{1 + k}\right)^{3/2}\frac{\frac{T_o + B}{T_o}}{\frac{1}{1 + k} + B} \tag{A4}$$

(This equation, of course, has the disadvantage in wind-tunnel work that, if the Mach number is high, the static temperature may be in the extremely low temperature range where experimental data are not available and have to be obtained from an extension of known data.)

Equation (A4) shows that the boundary-layer thicknesses are not the simple functions of Mach number and free-stream Reynolds number which are obtained from the power·formula for viscosity where

$$\frac{\mu_o}{\mu_\delta} = \left(\frac{T_o}{T_\delta}\right)^n \tag{A5}$$

and

$$\frac{\rho_\delta U}{\mu_o} = \frac{\rho_\delta U}{\mu_\delta}\left(\frac{1}{1 + k}\right)^n \tag{A6}$$

Equation (A5), in general, is only adequate over a relatively small range of temperature (though some few gases may be represented with good or better accuracy by this equation than by the formula of Sutherland); however, as the Mach number increases, the difference between free-stream temperature and stagnation temperature becomes large, and as the temperature range varies so does the power n for air and many gases. For example, at a Mach number of 7 and a free-stream temperature of -300° F, the stagnation temperature is 1269° F (when air is the medium), and for this large temperature difference the power formula is unsatisfactory.

For air, values of $A = 0.0220 \times 10^{-6}$ lb-sec/$(^\circ F)^{1/2}$-ft^2 and $B = 177^\circ$ F give errors of less than 1 percent in the range of temperature from 140° to 750° F absolute and an error of only $2\frac{1}{2}$ percent between 2000° and 3500° F absolute. These values have been used in the computation of the curves presented in figure 5; however, the values of $A = 0.0291 \times 10^{-6}$ lb-sec/$(^\circ F)^{1/2}$-ft^2 and $B = 198^\circ$ F obtained from reference 3 are somewhat better for temperatures above 250° F absolute. The magnitudes of these errors have been obtained from a comparison with experimental data obtained from references 15 to 19.

REFERENCES

1. Busemann, A.: Gasströmung mit laminarer Grenzschicht entlang einer Platte. Z.f.a.M.M., Bd. 15, Heft 1/2, Feb. 1935, pp. 23-25.

2. Von Kármán, Th., and Tsien, H. S.: Boundary Layer in Compressible Fluids. Jour. Aero. Sci., vol. 5, no. 6, Apr. 1938, pp. 227-232.

3. Van Driest, E. R.: Investigation of Laminar Boundary Layer in Compressible Fluids Using the Crocco Method. NACA TN 2597, 1952.

4. Crocco, Luigi: Lo Strato Limite Laminare nei Gas. (Laminar Boundary Layer in Gases.) Monografie Scientifiche di Aeronautica, Nr. 3, Oct. 1946.

5. Klunker, E. B., and McLean, F. Edward: Laminar Friction and Heat Transfer at Mach Numbers From 1 to 10. NACA TN 2499, 1951.

6. Lees, Lester, and Probstein, Ronald F.: Hypersonic Viscous Flow Over a Flat Plate. Rep. No. 195, Princeton Univ., Aero. Eng. Lab., Apr. 20, 1952.

7. Prandtl, L.: The Mechanics of Viscous Fluids. Vol. III of Aerodynamic Theory, div. G, W. F. Durand, ed., Julius Springer (Berlin), 1935, pp. 34-208.

8. Fluid Motion Panel of the Aeronautical Research Committee and Others: Modern Developments in Fluid Dynamics. Vols. I and II, S. Goldstein, ed., The Clarendon Press (Oxford), 1938.

9. Weil, H.: Effects of Pressure Gradient on Stability and Skin Friction in Laminar Boundary Layers in Compressible Fluids. Rep. No. R49A0533, Gen. Elec. Co., Apr. 1950.

10. Puckett, Allen E.: Final Report on the Model Supersonic Wind-Tunnel Project. Armor and Ord. Rep. No. A-269, OSRD No. 3569, Div. 2, NDRC, 1944.

11. McLellan, Charles H., Williams, Thomas W., and Bertram, Mitchel H.: Investigation of a Two-Step Nozzle in the Langley 11-Inch Hypersonic Tunnel. NACA TN 2171, 1950.

12. McLellan, Charles H., Williams, Thomas W., and Beckwith, Ivan E.: Investigation of the Flow Through a Single-Stage Two-Dimensional Nozzle in the Langley 11-Inch Hypersonic Tunnel. NACA TN 2223, 1950.

13. Becker, John V.: Results of Recent Hypersonic and Unsteady Flow Research at the Langley Aeronautical Laboratory. Jour. Appl. Phys., vol. 21, no. 7, July 1950, pp. 619-628.

14. McLellan, Charles H.: Exploratory Wind-Tunnel Investigation of Wings and Bodies at M = 6.9. Jour. Aero. Sci., vol. 18, no. 10, Oct. 1951, pp. 641-648.

15. Hodgman, Charles D., ed.: Handbook of Chemistry and Physics. Thirty-third ed., Chemical Rubber Publishing Co., 1951-1952.

16. Roth, Walther A., and Scheel, Karl, eds.: Landolt-Börnstein Physikalisch-Chemische Tabellen. Fifth ed., vol. 1. Julius Springer (Berlin), 1923.

17. Fowle, Frederick E., ed.: Smithsonian Physical Tables. Eighth rev. ed., Smithsonian Misc. Coll., vol. 88, 1933.

18. Johnston, Herrick L., and McCloskey, Kenneth E.: Viscosities of Several Common Gases Between 90°K. and Room Temperature. Jour. Phys. Chem., vol. 44, no. 9, Dec. 1940, pp. 1038-1058.

19. Vasilesco, Virgile: Recherches expérimentales sur la viscosité des gaz aux températures élevées. Chs. V-VIII, Ann. de Phys., vol. 20, ser. 11, May-June, 1945, pp. 292-334.

TABLE I

INTEGRAL TERM OF EQUATION (19)

M	$\int_0^M \frac{\theta}{\delta} \frac{M^9 dM}{\left(5 + M^2\right)^{3.60}}$
0	0
1.00	.000047
1.25	.000203
1.50	.000789
2.00	.006489
3.00	.06779
4.00	.2432
5.00	.5592
6.00	.9957
7.00	1.525
8.00	2.118
9.00	2.760
10.00	3.440

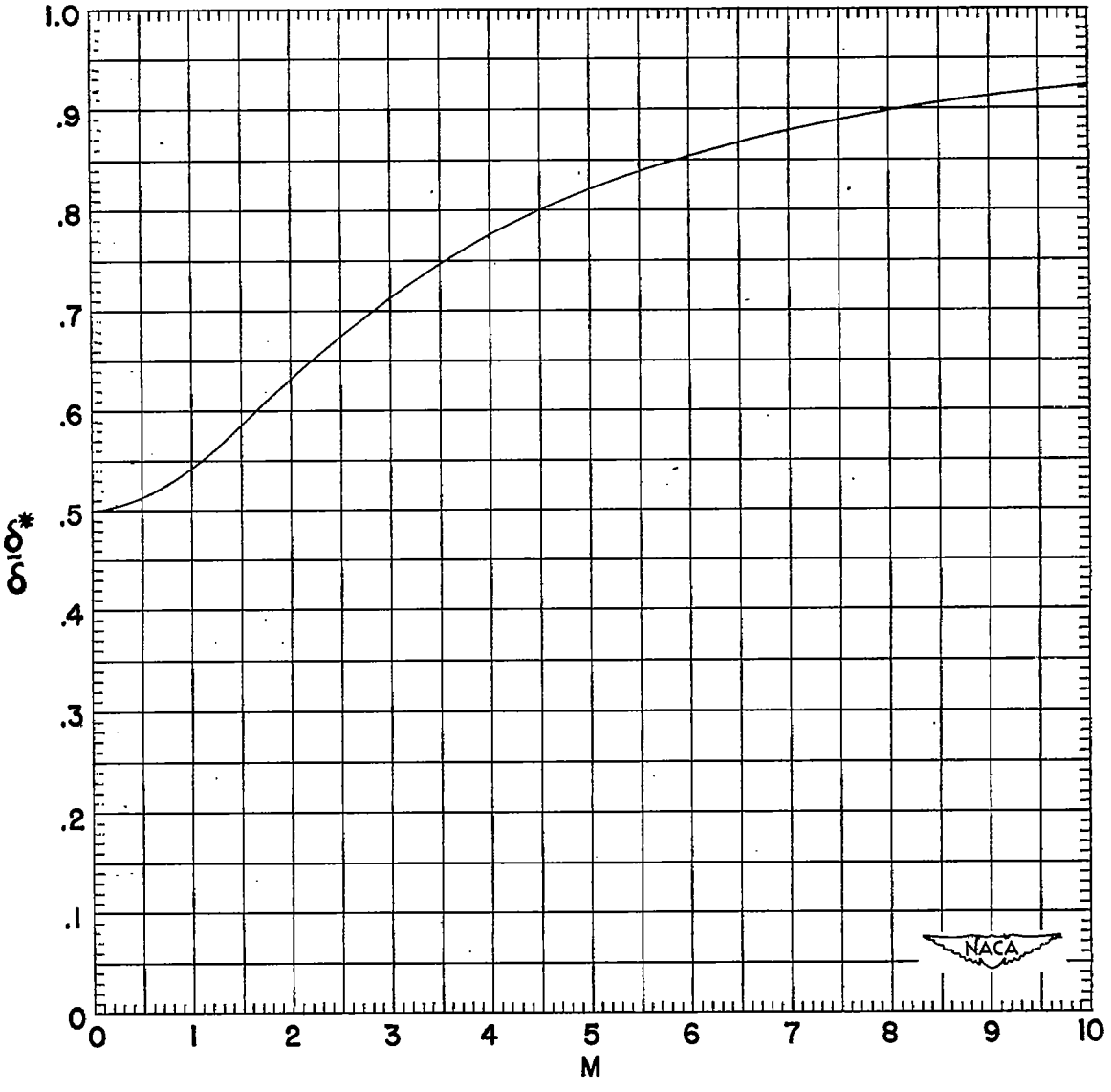

Figure 1 .— Ratio of boundary-layer displacement thickness to total thickness as a function of the Mach number at the edge of the boundary layer where the velocity distribution across the boundary layer is linear.

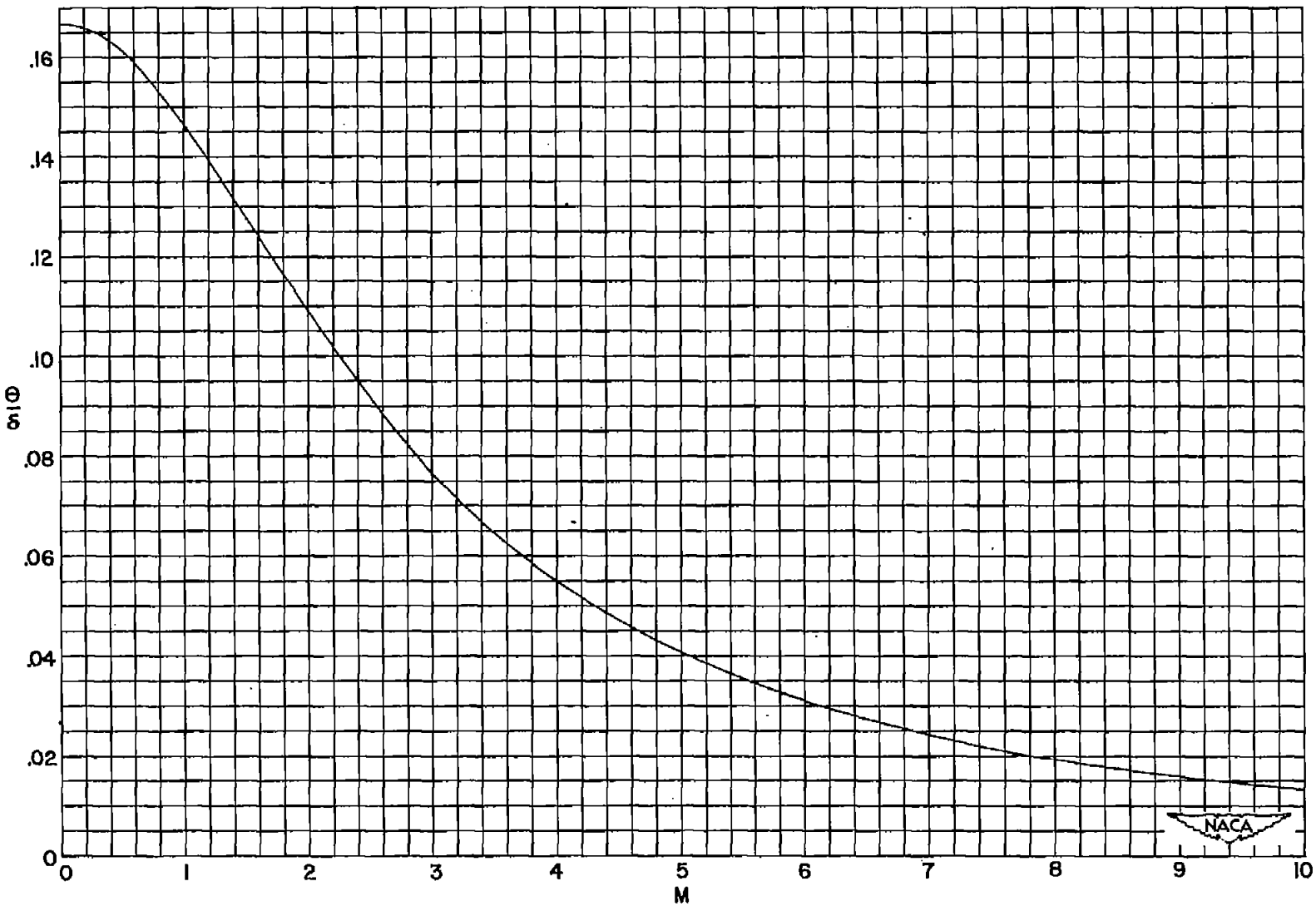

Figure 2 .-- Ratio of the boundary-layer momentum thickness to total thickness as a function of the Mach number at the edge of the boundary layer where the velocity distribution across the boundary layer is linear.

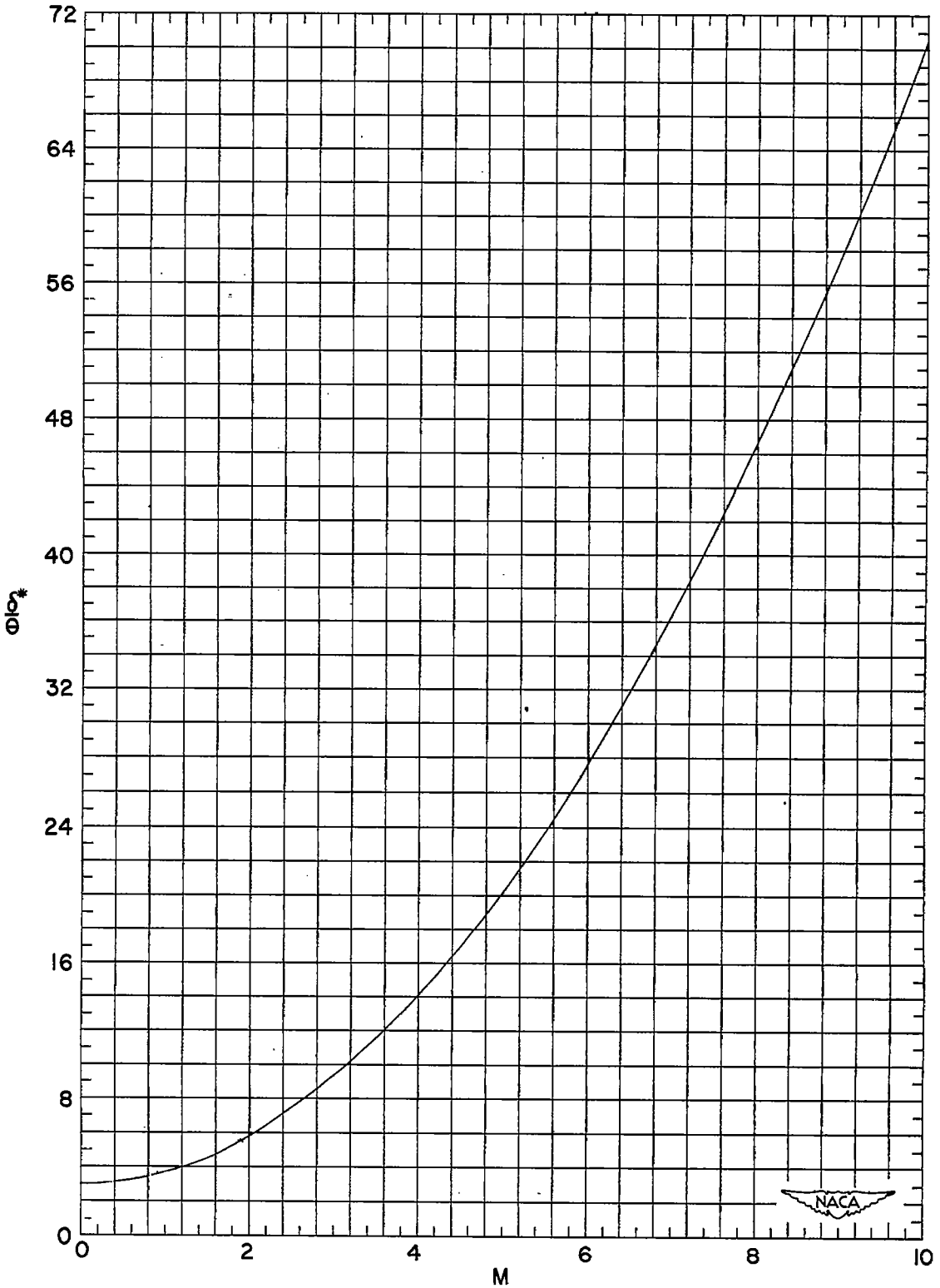

Figure 3 .— Ratio of the boundary-layer displacement thickness to momentum thickness as a function of the Mach number at the edge of the boundary layer where the velocity distribution across the boundary layer is linear.

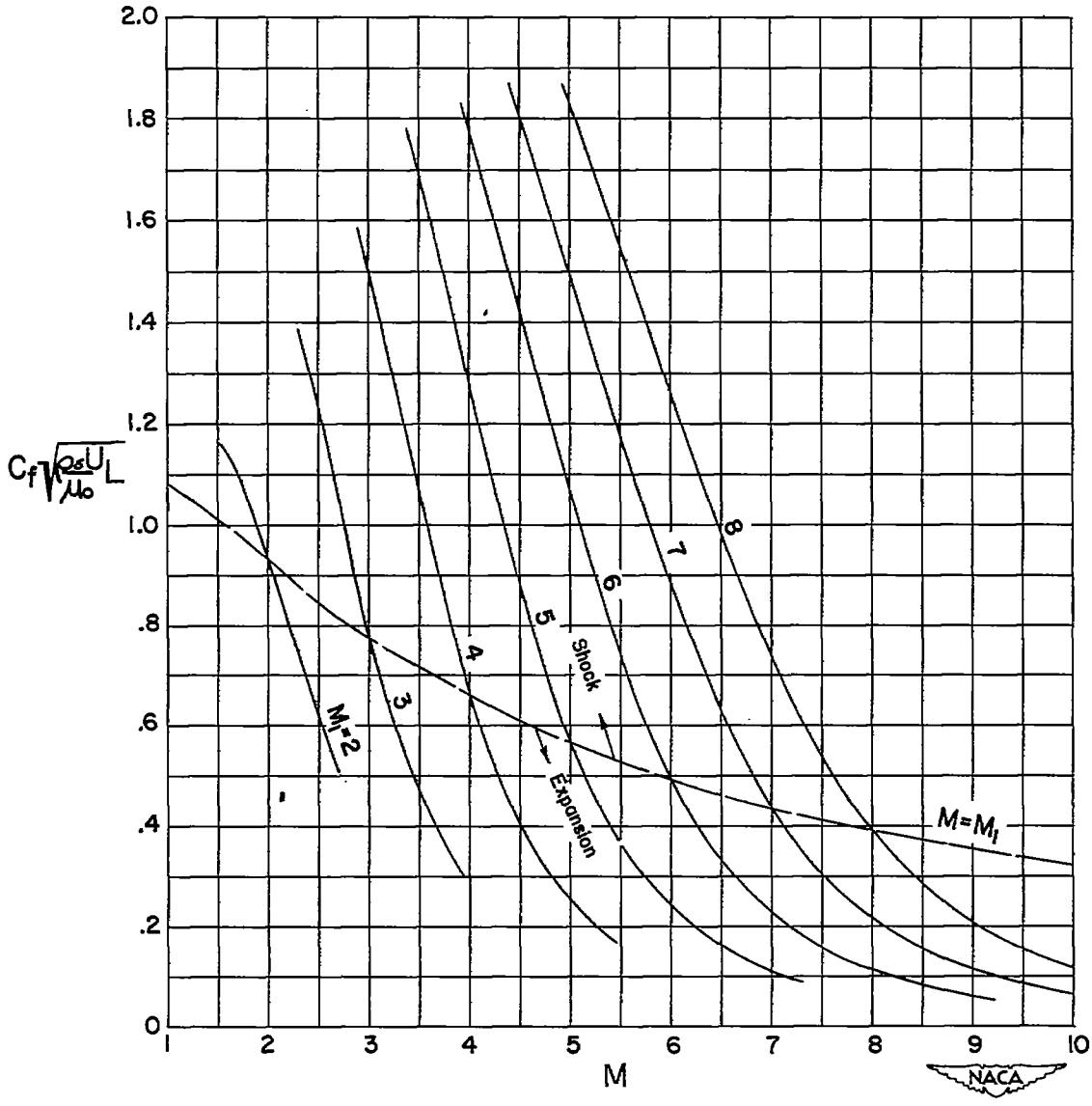

Figure 4.- The skin friction for one side of a flat plate in supersonic flow where the free-stream Mach number over the plate is varied (corresponding to varying angle of attack) and the free-stream Mach number before the plate is maintained constant.

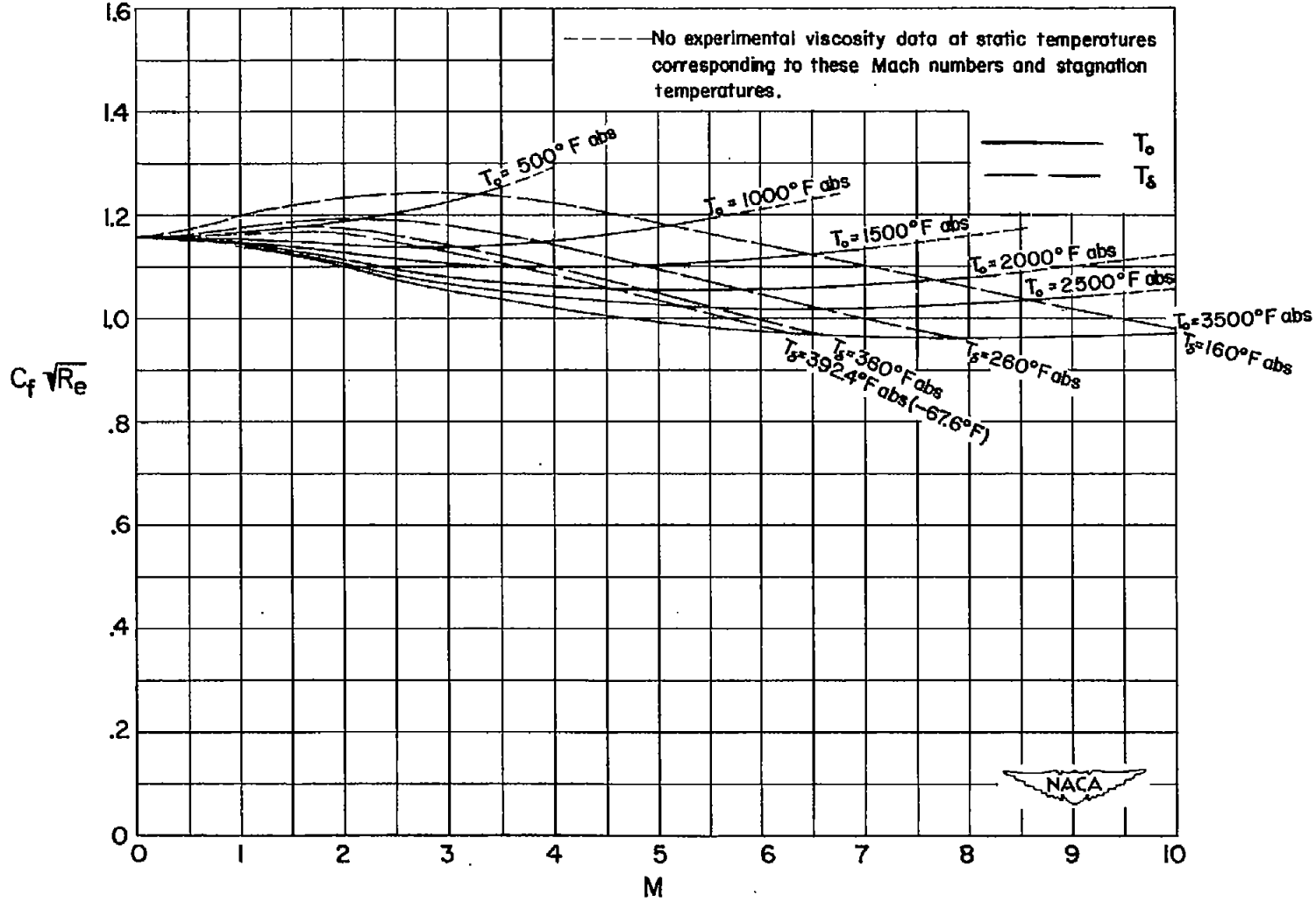

Figure 5 .— The skin friction for one side of a flat plate at various temperatures where the conditions in the free stream over the plate are the same as those in the free stream before the plate.

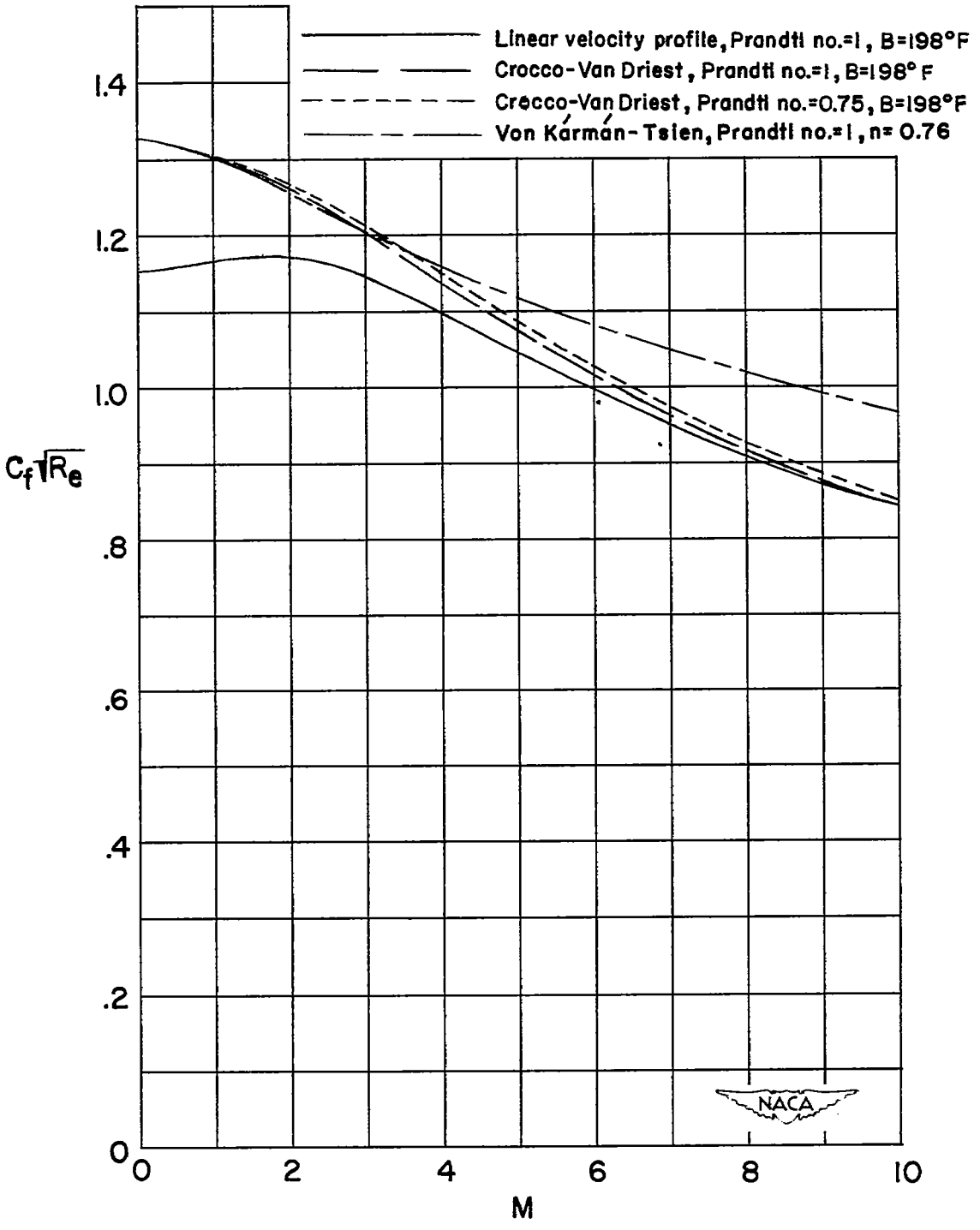

Figure 6.—Comparison of skin-friction coefficients for an insulated flat plate computed from several theories for a free-stream temperature of -67.6° F.

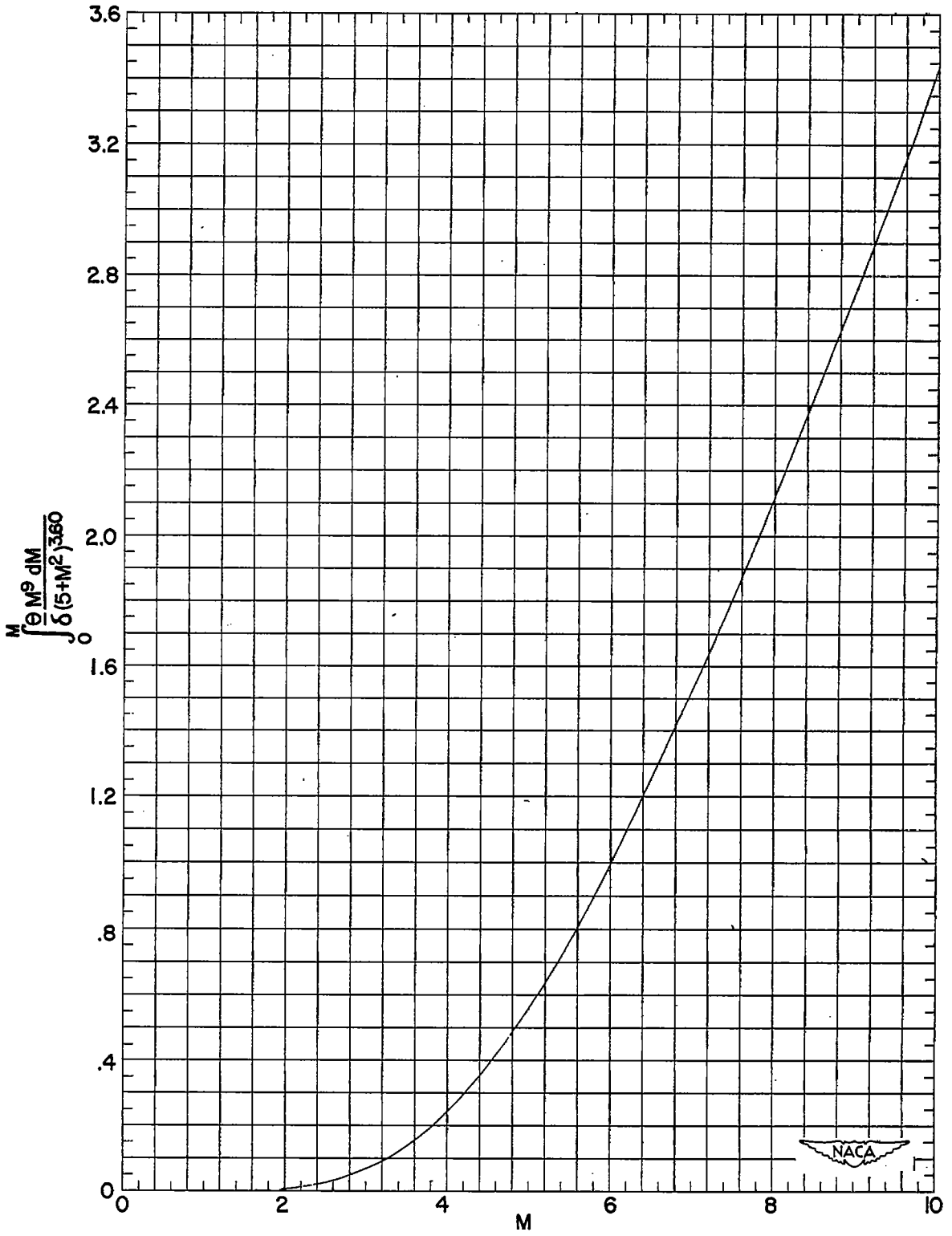

Figure 7 .—Value from 0 to M of the integral in the momentum-thickness equation with pressure gradient as a function of Mach number where the velocity distribution across the boundary layer is linear.

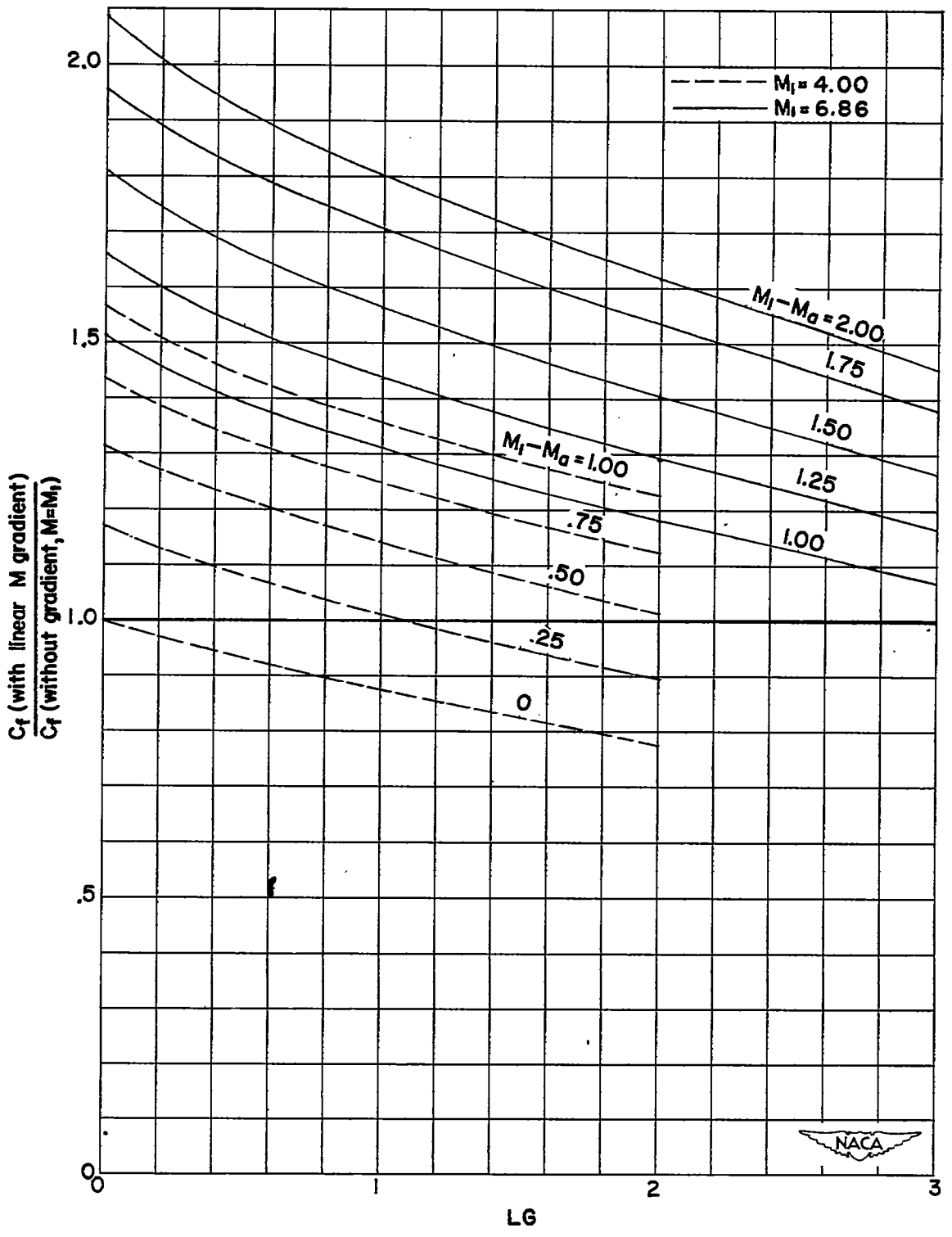

Figure 8.– The skin-friction coefficient of a plate with a constant Mach number gradient compared with that of a flat plate (with $M=M_l$) where M_a is the Mach number immediately following the shock at the leading edge of the plate with the Mach number gradient.

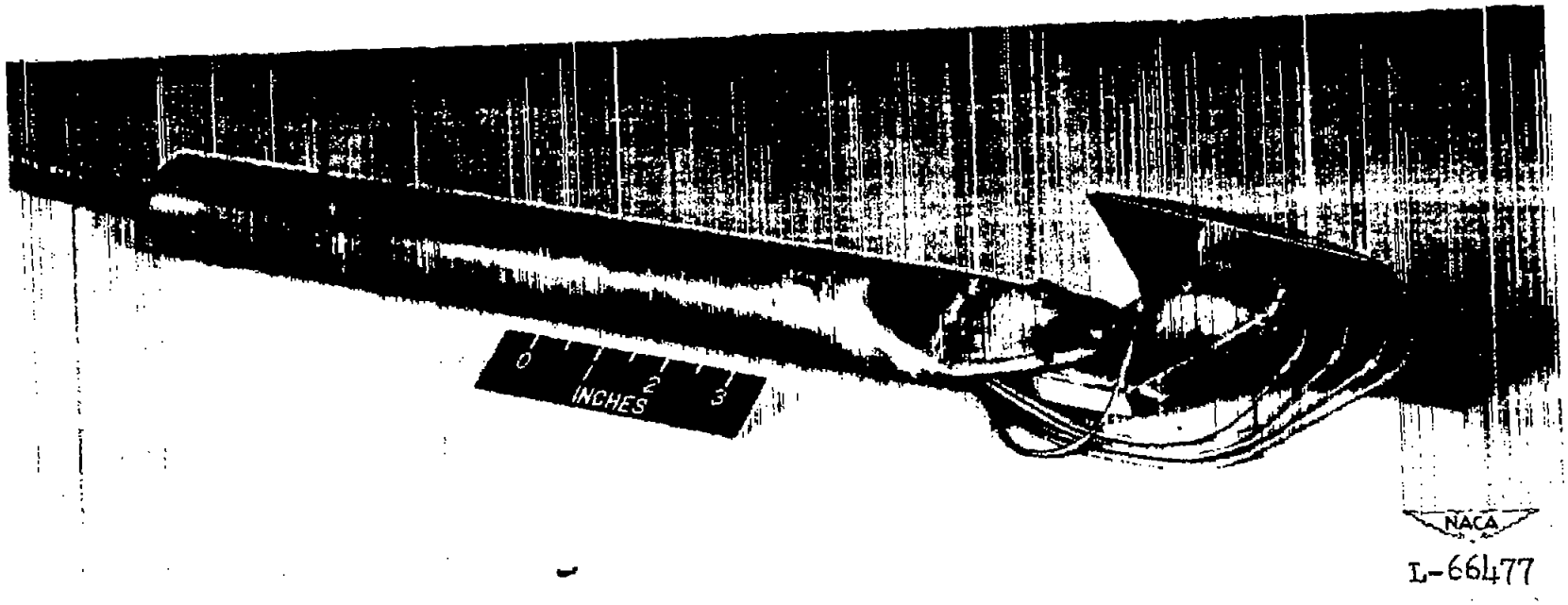

Figure 9.- View of circular-arc surface mounted on its support sting with pressure tubing protruding from the flat undersurface.

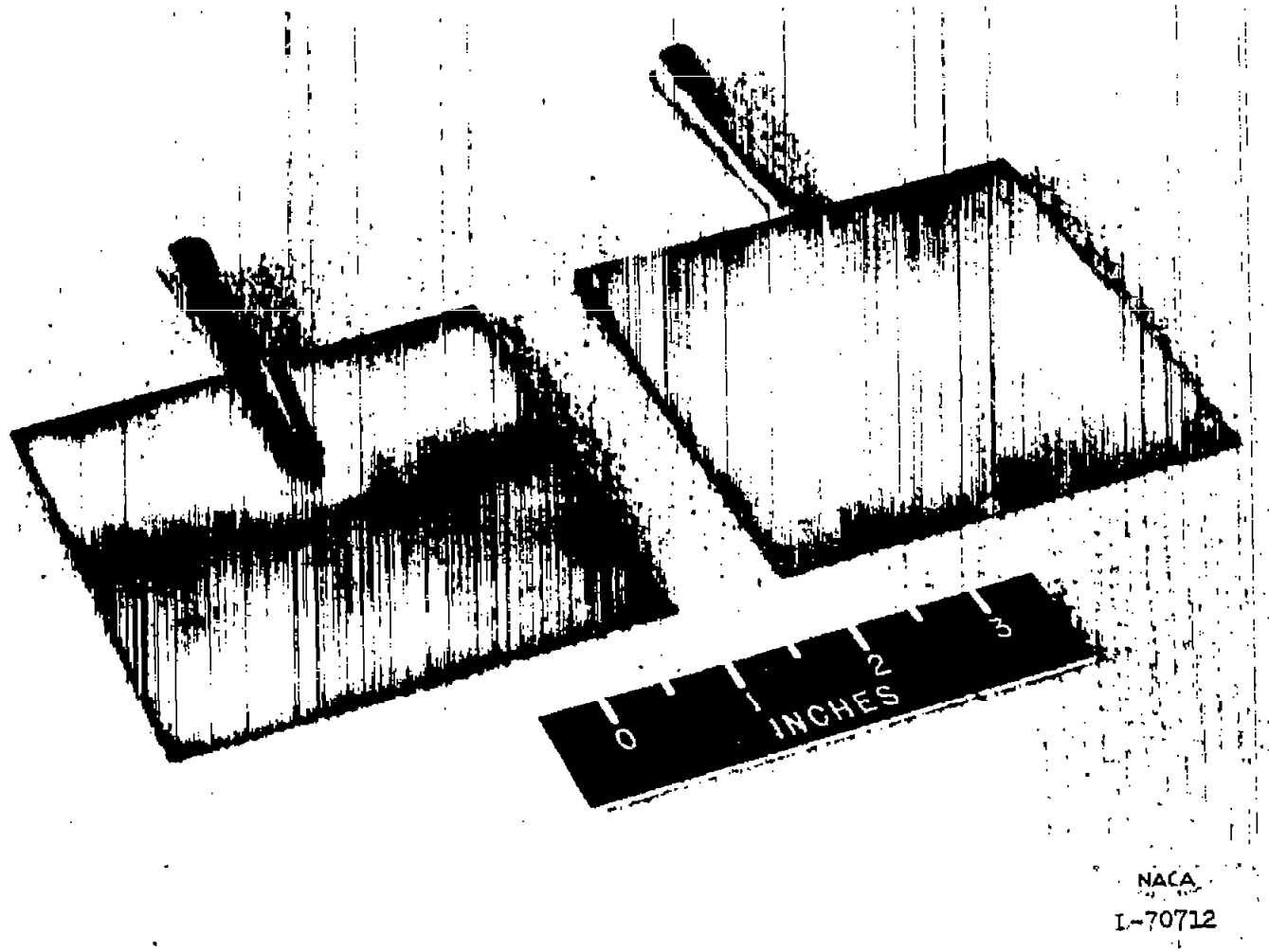

Figure 10.- Diamond-section and wedge-section 5-percent-thick square-planform force models.

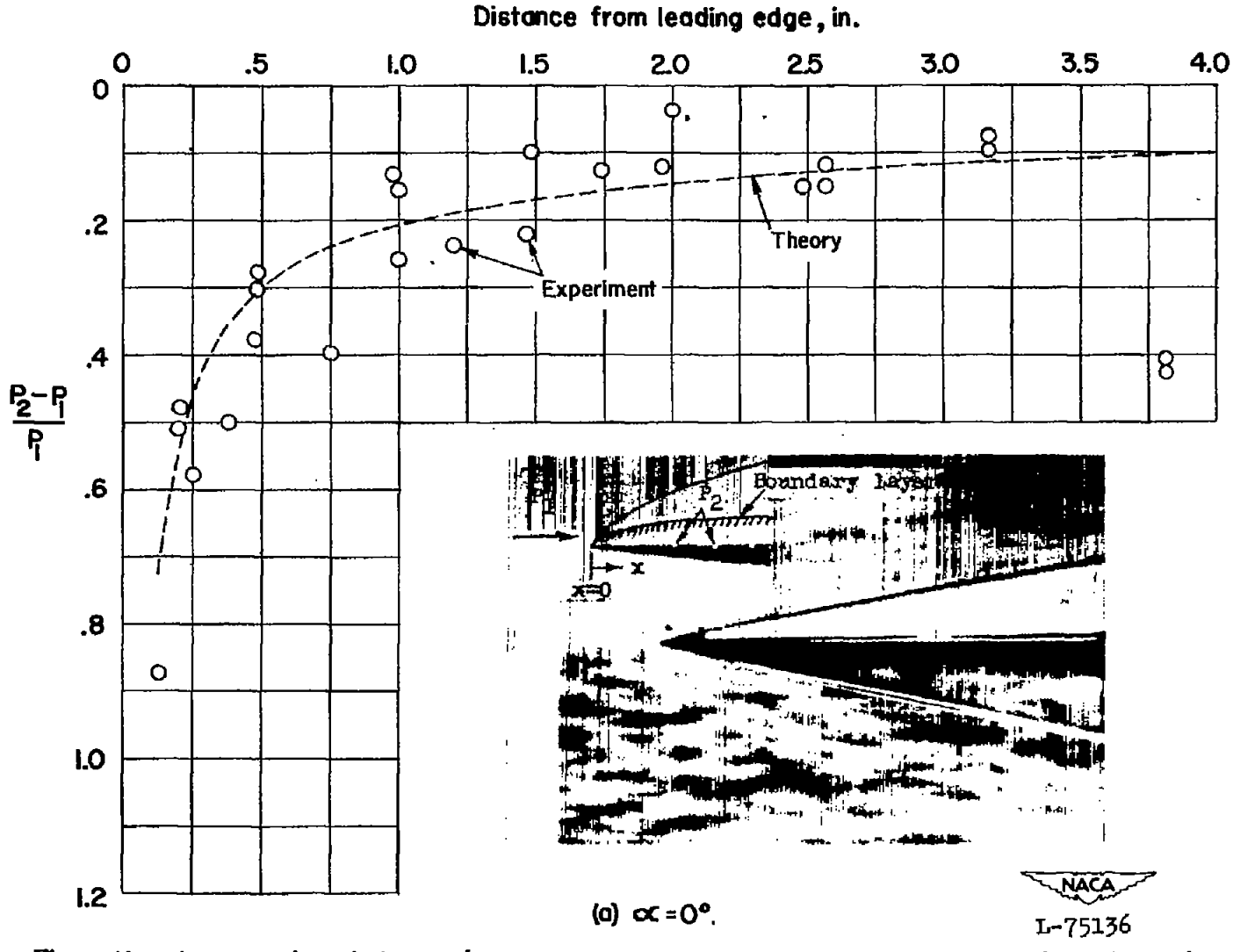

(a) $\alpha = 0°$.

Figure 11.– A comparison between theoretical and experimental pressures over a flat plate where the flow is initially at $M = 6.86$ and $R_e = 0.98 \times 10^6$.

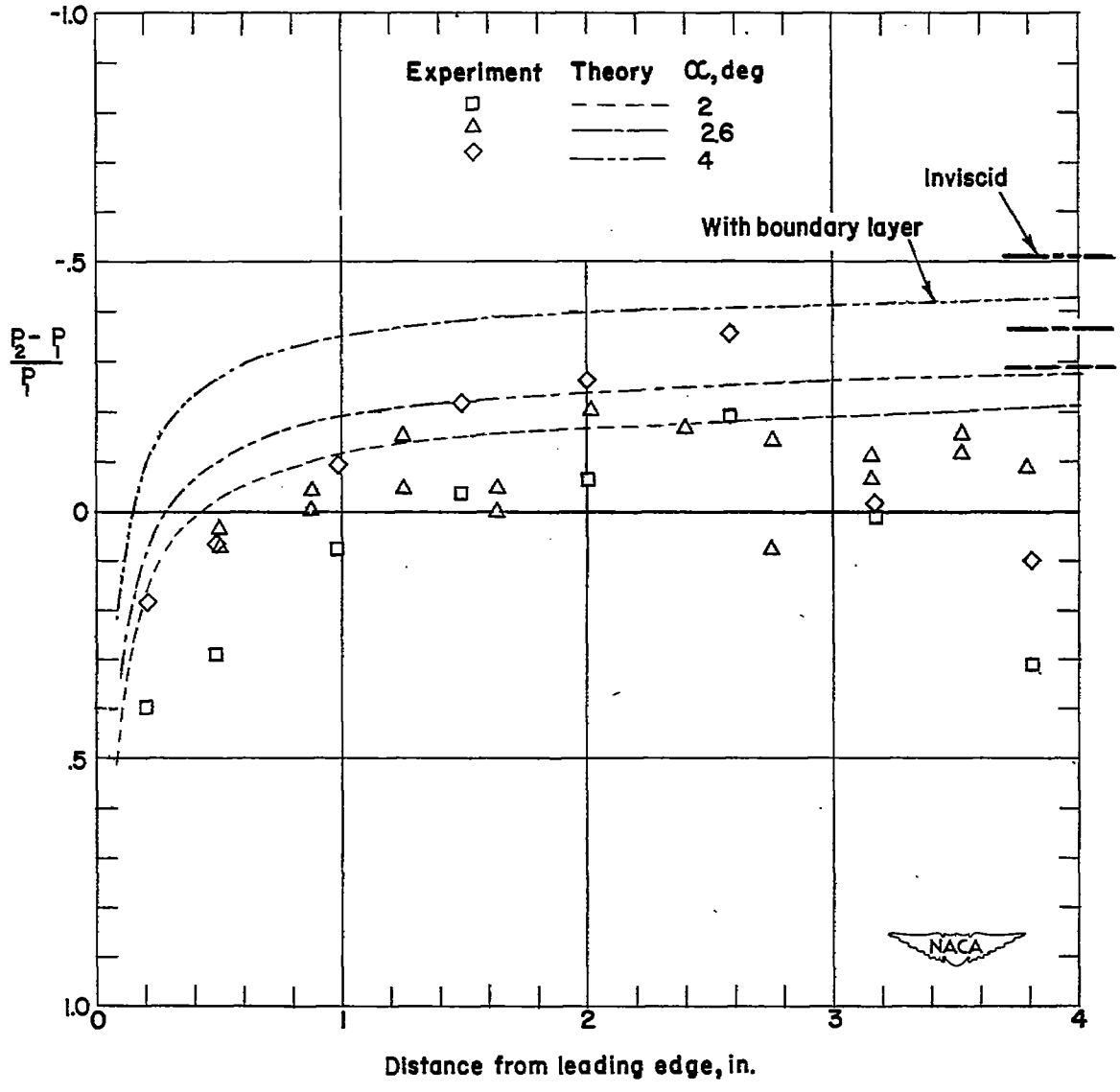

(b) Upper surface.

Figure 11.– Continued.

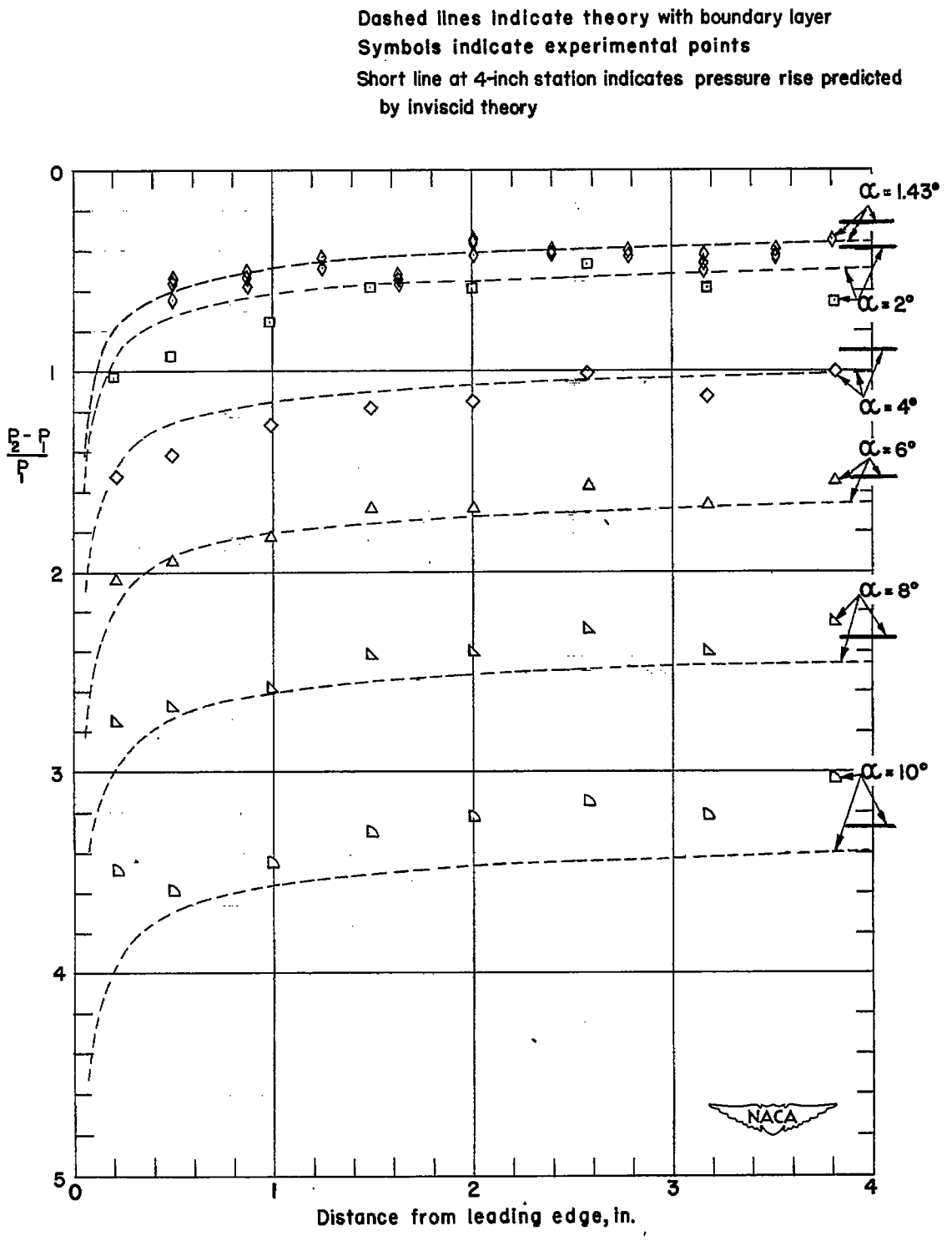

(c) Lower surface.

Figure 11.—Concluded.

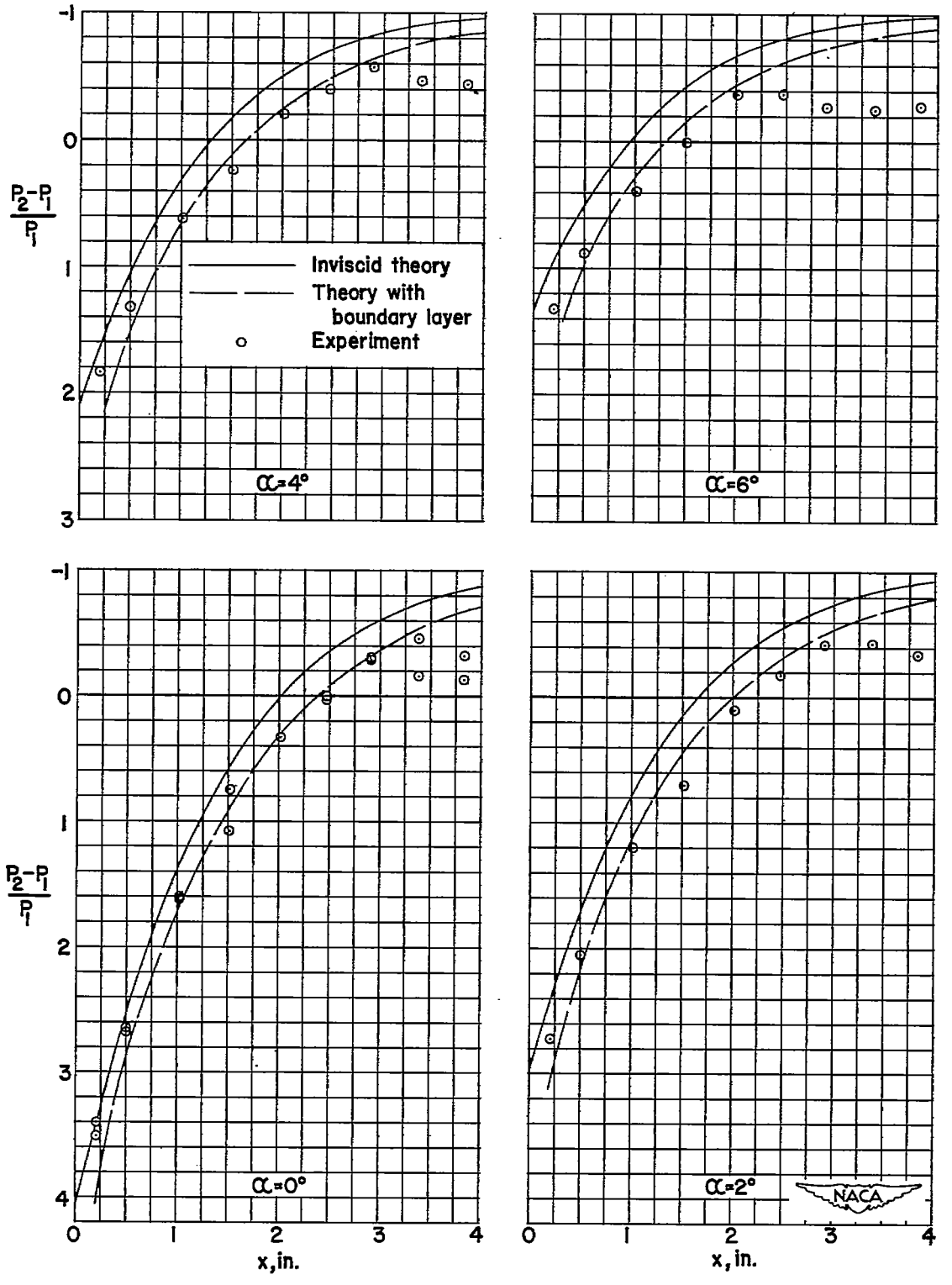

Figure 12 .— A comparison between the theoretical and experimental pressure distribution over a circular arc surface where the flow is initially at M=6.86 and R_δ=0.98x10^6.

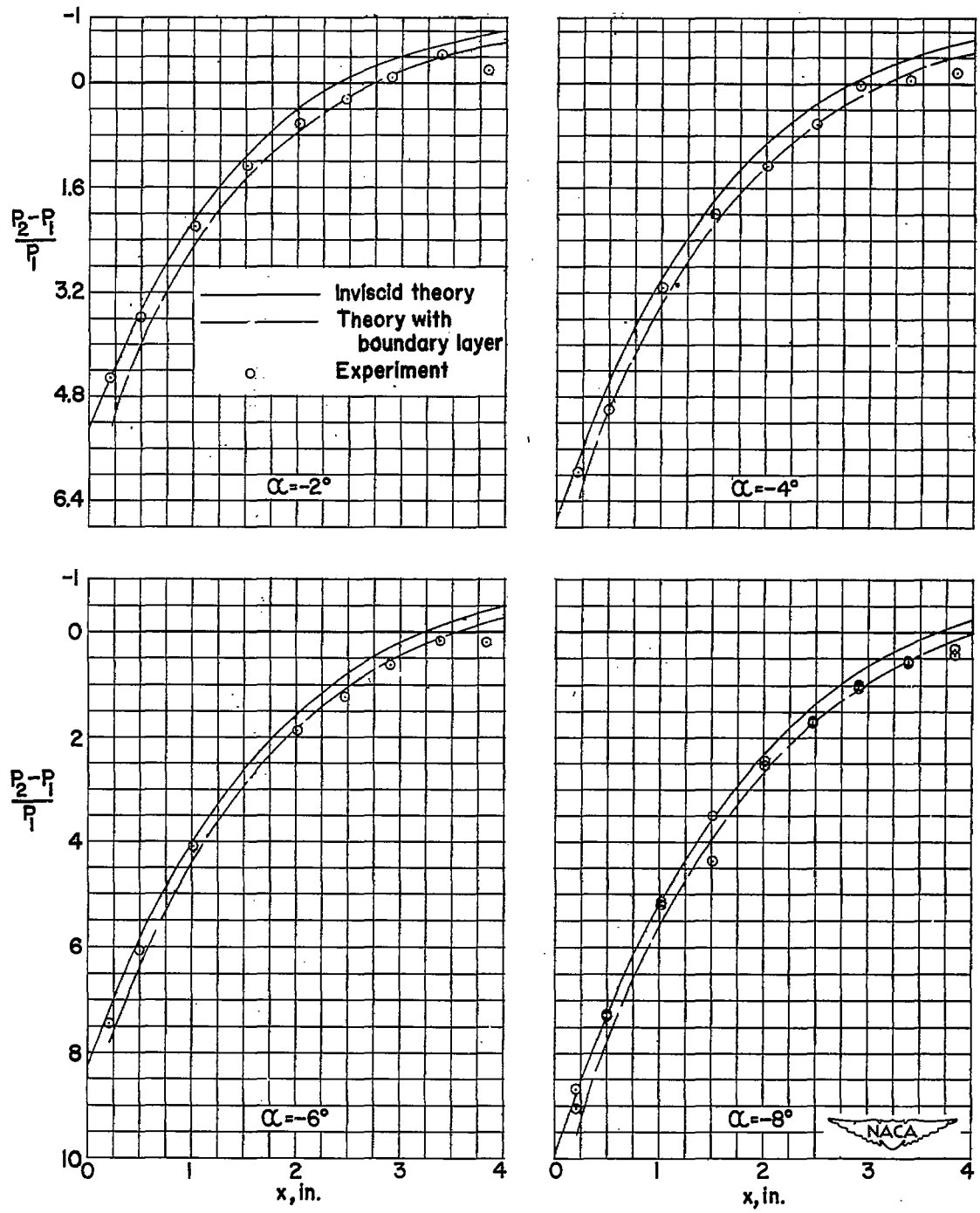

Figure 12.–Concluded.

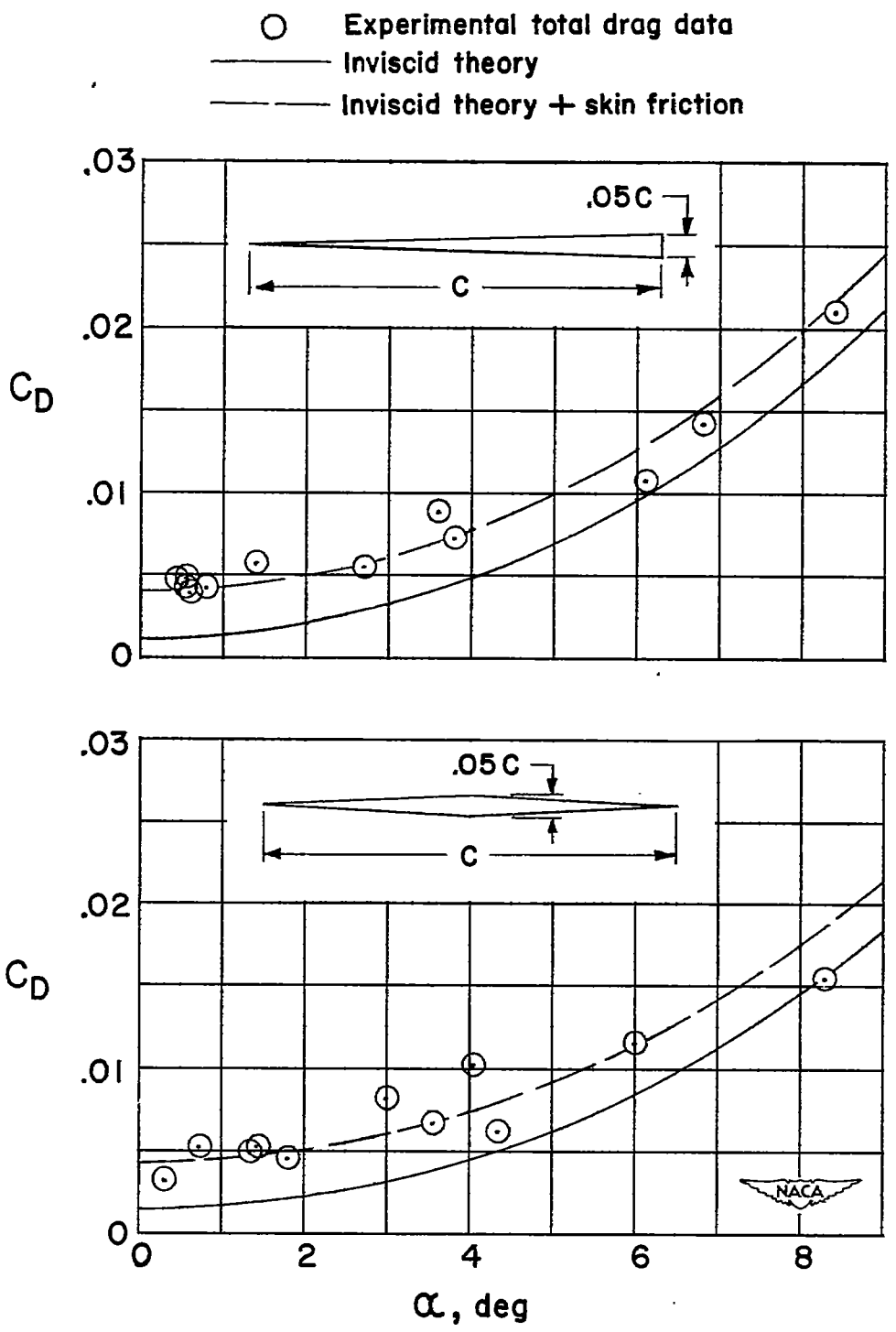

Figure 13.– A comparison between the experimental and theoretical drag coefficients of two square plan-form models. M=6.86 and $R_e = 0.98 \times 10^6$.